ORIGIN AND PROPAGATION OF THE HIGHEST ENERGY COSMIC RAYS

R.J. PROTHEROE

Department of Physics and Mathematical Physics
The University of Adelaide, Adelaide, Australia 5005

ABSTRACT

In this lecture I give an overview of shock acceleration, interactions of high energy cosmic rays with, and propagation through, the background radiation, and the resulting electron-photon cascade. I argue that while the origin of the highest energy cosmic rays is still uncertain, it is not necessary to invoke exotic models such as emission by topological defects to explain the existing data. It seems likely that shock acceleration at Fanaroff-Riley Class II radio galaxies can account for the existing data. However, new cosmic ray data, as well as better estimates of the extragalactic radiation fields and magnetic fields will be necessary before we will be certain of the origin of the highest energy particles occurring in nature.

1 Introduction

Cosmic rays with energies up to 100 TeV are thought to arise predominantly through shock acceleration by supernova remnants (SNR) in our Galaxy [1]. A fraction of the cosmic rays accelerated should interact within the supernova remnant and produce gamma–rays [2, 3], and recent observations above 100 MeV by the EGRET instrument on the Compton Gamma Ray Observatory have found gamma ray signals associated with at least two supernova remnants – IC 443 and γ Cygni [4] (however, it is possible that the gamma ray emission from IC 443 is associated with a pulsar within the remnant rather than the remnant itself [5]). Further evidence for acceleration in SNR comes from the recent ASCA observation of non-thermal X–ray emission from SN 1006 [6]. Reynolds [7] and Mastichiadis [8] interpret the latter as synchrotron emission by electrons accelerated in the remnant up to energies as high as 100 TeV, although Donau and Biermann [9] suggest it may be bremsstrahlung from much lower energy electrons.

Acceleration to somewhat higher energies than 100 TeV may be possible [10], but probably not high enough to explain the smooth extension of the spectrum to 1 EeV. Several explanations for the origin of the cosmic rays in this energy range have been suggested: reacceleration of the supernova component while still inside the remnant [11]; by several supernovae exploding into a region evacuated by a pre-supernova star [12]; or acceleration in shocks inside the strong winds from hot stars or groups of hot stars [13]. At 5 EeV the spectral slope changes, and there is evidence for a lightening in composition [14]

and it is likely this marks a change from galactic cosmic rays to extragalactic cosmic rays being dominant.

The cosmic ray air shower events with the highest energies so far detected have energies of 2×10^{11} GeV [15] and 3×10^{11} GeV [16]. The question of the origin of these cosmic rays having energy significantly above 10^{11} GeV is complicated by propagation of such energetic particles through the universe. Nucleons interact with the cosmic background radiation fields, losing energy by pion photoproduction, and may emerge as either protons or neutrons with reduced energy. The threshold for pion photoproduction on the microwave background is $\sim 2 \times 10^{10}$ GeV, and at 3×10^{11} GeV the energy-loss distance is about 20 Mpc. Propagation of cosmic rays over substantially larger distances gives rise to a cut-off in the spectrum at $\sim 10^{11}$ GeV as was first shown by Greisen [17], and Zatsepin and Kuz'min [18], the "GZK cut-off", and a corresponding pile-up at slightly lower energy [19, 20]. These processes occur not only during propagation, but also during acceleration and may actually limit the maximum energies particles can achieve.

In this lecture I give an overview of shock acceleration, describe interactions of high energy protons and nuclei with radiation, discuss maximum energies obtainable during acceleration, outline propagation of cosmic rays through the background radiation and the consequent electron-photon cascading, and finally discuss conventional and exotic models of the highest energy cosmic rays.

2 Cosmic Ray Acceleration

For stochastic particle acceleration by electric fields induced by motion of magnetic fields B, the rate of energy gain by relativistic particles of charge Ze can be written (in SI units)

$$\left. \frac{dE}{dt} \right|_{\mathrm{acc}} = \xi Z e c^2 B \tag{1}$$

where $\xi < 1$ and depends on the acceleration mechanism. I shall give a simple heuristic treatment of Fermi acceleration based on that given in Gaisser's excellent book [21]. I shall start with 2nd order Fermi acceleration (Fermi's original theory) and describe how this can be modified in the context of supernova shocks, or other strong astrophysical shocks, into the more efficient 1st order Fermi mechanism at supernova (SN) or other shocks. More detailed and rigorous treatments are given in several review articles [22–25]. See the review by Jones and Ellison [25] on the plasma physics of shock acceleration which also includes a brief historical review and refers to early work.

Gas clouds in the interstellar medium have random velocities of ~ 15 km/s superimposed on their regular motion around the galaxy. Cosmic rays gain energy on average when scattering off these magnetized clouds. A cosmic ray enters a cloud and scatters off irregularities in the magnetic field which is tied to the cloud because it is partly ionized.

In the frame of the cloud: (a) there is no change in energy because the scattering is collisionless, and so there is elastic scattering between the cosmic ray and the cloud as a whole which is much more massive than the cosmic ray; (b) the cosmic ray's direction is randomized by the scattering and it emerges from the cloud in a random direction.
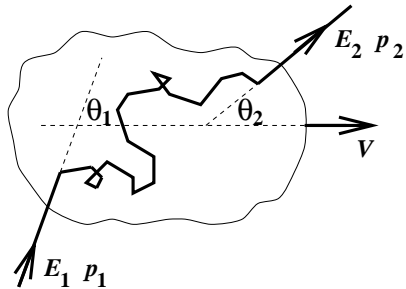

Figure 1: Interaction of cosmic ray of energy E_1 with "cloud" moving with speed V

Consider a cosmic ray entering a cloud with energy E_1 and momentum p_1 travelling in a direction making angle θ_1 with the cloud's direction. After scattering inside the cloud, it emerges with energy E_2 and momentum p_2 at angle θ_2 to the cloud's direction (Fig. 1). The energy change is obtained by applying the Lorentz transformations between the laboratory frame (unprimed) and the cloud frame (primed). Transforming to the cloud frame:

$$E_1' = \gamma E_1 (1 - \beta \cos \theta_1) \tag{2}$$

where $\beta = V/c$ and $\gamma = 1/\sqrt{1 - \beta^2}$.
Transforming to the laboratory frame:

$$E_2 = \gamma E_2' (1 + \beta \cos \theta_2'). \tag{3}$$

Since $E_2' = E_1'$ we obtain the fractional change in energy $(E_2 - E_1)/E_1$,

$$\frac{\Delta E}{E} = \frac{1 - \beta \cos \theta_1 + \beta \cos \theta_2' - \beta^2 \cos \theta_1 \cos \theta_2'}{1 - \beta^2} - 1. \tag{4}$$

We need to obtain average values of $\cos\theta_1$ and $\cos\theta_2'$. Inside the cloud, the cosmic ray scatters off magnetic irregularities many times so that its direction is randomized,

$$\langle\cos\theta_2'\rangle = 0. \tag{5}$$

The average value of $\cos\theta_1$ depends on the rate at which cosmic rays collide with clouds at different angles. The rate of collision is proportional to the relative velocity between the cloud and the particle so that the probability per unit solid angle of having a collision at angle θ_1 is proportional to $(v - V\cos\theta_1)$. Hence, for ultrarelativistic particles $(v = c)$

$$\frac{dP}{d\Omega_1} \propto (1 - \beta\cos\theta_1), \tag{6}$$

and we obtain

$$\langle\cos\theta_1\rangle = \int \cos\theta_1 \frac{dP}{d\Omega_1} d\Omega_1 / \int \frac{dP}{d\Omega_1} d\Omega_1 = -\frac{\beta}{3}, \tag{7}$$

giving

$$\frac{\langle\Delta E\rangle}{E} = \frac{1 + \beta^2/3}{1 - \beta^2} - 1 \simeq \frac{4}{3}\beta^2 \tag{8}$$

since $\beta \ll 1$.

We see that $\langle\Delta E\rangle/E \propto \beta^2$ is positive (energy gain), but is 2nd order in β and because $\beta \ll 1$ the average energy gain is very small. This is because there are almost as many overtaking collisions (energy lost) as there are head-on collisions (energy gain).

2.2   1st Order Fermi Acceleration at SN or Other Shocks

Fermi's original theory was modified in the 1970's [26–29] to describe more efficient acceleration (1st order in β) taking place at supernova shocks but is generally applicable to strong shocks in other astrophysical contexts.

During a supernova explosion several solar masses of material are ejected at a speed of $\sim 10^4$ km/s which is much faster than the speed of sound in the interstellar medium (ISM) which is ~ 10 km/s. A strong shock wave propagates radially out as the ISM and its associated magnetic field piles up in front of the supernova ejecta. The velocity of the shock, V_S, depends on the velocity of the ejecta, V_P, and on the ratio of specific heats, γ. The SN will have ionized the surrounding gas which will therefore be monatomic ($\gamma = 5/3$), and theory of shock hydrodynamics shows that for a strong shock

$$V_S/V_P \simeq 4/3. \tag{9}$$

4

In order to work out the energy gain per shock crossing, we can visualize magnetic irregularities on either side of the shock as clouds of magnetized plasma of Fermi's original theory (Fig. 2). By considering the rate at which cosmic rays cross the shock from downstream to upstream, and upstream to downstream, one finds $\langle \cos \theta_1 \rangle = -2/3$ and $\langle \cos \theta_2' \rangle = 2/3$, giving

$$\frac{\langle \Delta E \rangle}{E} \simeq \frac{4}{3}\beta \simeq \frac{V_S}{c}. \tag{10}$$

Note this is 1st order in β and is therefore more efficient than Fermi's original theory. This is because of the converging flow – whichever side of the shock you are on, if you are moving with the plasma, the plasma on the other side of the shock is approaching you at speed V_p.
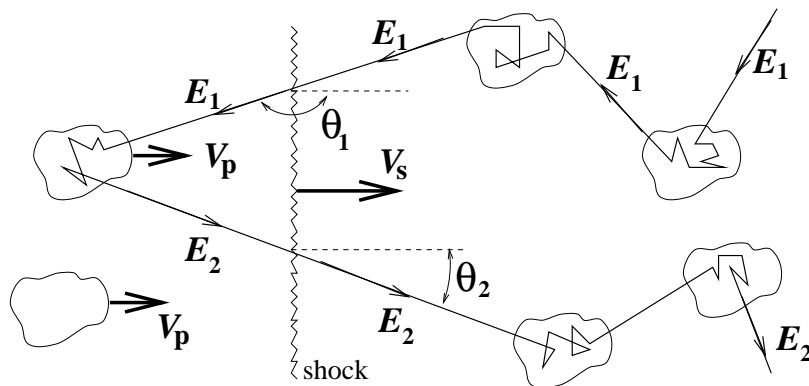

Figure 2: Interaction of cosmic ray of energy E_1 with a shock moving with speed V_s.

To obtain the energy spectrum we need to find the probability of a cosmic ray encountering the shock once, twice, three times, etc. If we look at the diffusion of a cosmic ray as seen in the rest frame of the shock (Fig. 3), there is clearly a net flow of the energetic particle population in the downstream direction. The net flow rate gives the rate at which cosmic rays are lost downstream

$$R_{\text{loss}} = n_{\text{CR}} V_S / 4 \qquad \text{m}^{-2}\text{s}^{-1} \tag{11}$$

since cosmic rays with number density n_{CR} at the shock are advected downstream with speed $V_S/4$ (from right to left in Fig. 3).

Upstream of the shock, cosmic rays travelling at speed v at angle θ to the shock normal (as seen in the laboratory frame) approach the shock with speed $(V_S + v \cos \theta)$ as seen in the shock frame. Clearly, to cross the shock,
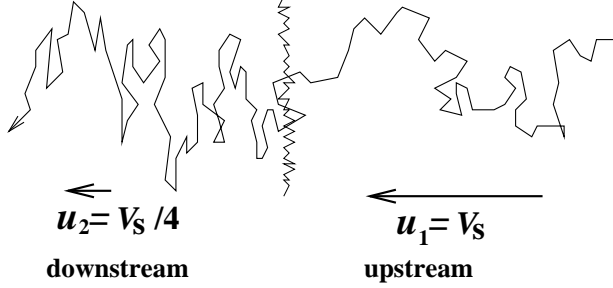
5

Figure 3: Diffusion of cosmic rays from upstream to downstream seen in the shock frame speed V_s.

$\cos\theta > -V_S/v$. Then, assuming cosmic rays upstream are isotropic, the rate at which they cross from upstream to downstream is

$$R_{\rm cross} = n_{\rm CR}\frac{1}{4\pi}\int_{-V_S/v}^{1}(V_S + v\cos\theta)2\pi d(\cos\theta) = n_{\rm CR}v/4 \quad {\rm m}^{-2}{\rm s}^{-1}. \quad (12)$$

The probability of crossing the shock once and then escaping from the shock (being lost downstream) is the ratio of these two rates:

$$\text{Prob.(escape)} = R_{\rm loss}/R_{\rm cross} = V_S/v \qquad (13)$$

where we have neglected relativistic transformations of the rates because $V_S \ll c$. The probability of returning to the shock after crossing from upstream to downstream is

$$\text{Prob.(return)} = 1 - \text{Prob.(escape)} \qquad (14)$$

and so the probability of returning to the shock k times and also of crossing the shock at least k times is

$$\text{Prob.(cross} \geq k) = [1 - \text{Prob.(escape)}]^k. \qquad (15)$$

Hence, the energy after k shock crossings is

$$E = E_0\left(1 + \frac{\Delta E}{E}\right)^k \qquad (16)$$

where E_0 is the initial energy.

To derive the spectrum, we note that the integral energy spectrum (number of particles with energy greater than E) on acceleration must be

$$Q(> E) \propto [1 - \text{Prob.(escape)}]^k \qquad (17)$$

6

where

$$k = \frac{\ln(E/E_0)}{\ln(1 + \Delta E/E)}. \tag{18}$$

Hence,

$$\ln Q(> E) = A + \frac{\ln(E/E_0)}{\ln(1 + \Delta E/E)} \ln[1 - \text{Prob.(escape)}], \tag{19}$$

where A is a constant, and so

$$\ln Q(> E) = B - \Gamma \ln E \tag{20}$$

where B is a constant and

$$\Gamma = -\frac{\ln[1 - \text{Prob.(escape)}]}{\ln(1 + \Delta E/E)} \approx 1. \tag{21}$$

Hence we arrive at the spectrum of cosmic rays on acceleration

$$Q(> E) \propto E^{-1} \qquad \text{(integral form)} \tag{22}$$

$$Q(E) \propto E^{-2} \qquad \text{(differential form).} \tag{23}$$

The observed cosmic ray spectrum is steepened by energy-dependent escape of cosmic rays from the Galaxy.

2.3   Shock Acceleration Rate

The rate of gain of energy is given by

$$\left. \frac{dE}{dt} \right|_{\text{acc}} = \frac{\Delta E}{t_{\text{cycle}}} \tag{24}$$

where t_{cycle} is the time for one complete cycle, i.e. from crossing the shock from upstream to downstream, diffusing back towards the shock and crossing from downstream to upstream, and finally returning to the shock. We shall discuss this process in the shock frame (see Fig. 3) and consider first particles crossing the shock from upstream to downstream and diffusing back to the shock, i.e. we shall work out the average time spent downstream. Since we are considering non-relativistic shocks, the time scales are approximately the same in the upstream and downstream plasma frames, and so in this section I shall drop the use of subscripts indicating the frame of reference.

Diffusion takes place in the presence of advection at speed u_2 in the downstream direction. The typical distance a particle diffuses in time t is $\sqrt{k_2 t}$ where k_2 is the diffusion coefficient in the downstream region. The distance

advected in this time is simply $u_2 t$. If $\sqrt{k_2 t} \gg u_2 t$ the particle has a very high probability of returning to the shock, and if $\sqrt{k_2 t} \ll u_2 t$ the particle has a very high probability of never returning to the shock (i.e. it has effectively escaped downstream). So, we set $\sqrt{k_2 t} = u_2 t$ to define a distance k_2/u_2 downstream of the shock which is effectively a boundary between the region closer to the shock where the particles will usually return to the shock and the region farther from the shock in which the particles will usually be advected downstream never to return. There are $n_{\mathrm{CR}} k_2/u_2$ particles per unit area of shock between the shock and this boundary. Dividing this by R_{cross} we obtain the average time spent downstream before returning to the shock

$$t_2 \approx \frac{4}{c} \frac{k_2}{u_2}. \tag{25}$$

Consider next the other half of the cycle after the particle has crossed the shock from downstream to upstream until it returns to the shock. In this case we can define a boundary at a distance k_1/u_1 upstream of the shock such that nearly all particles upstream of this boundary have never encountered the shock, and nearly all the particles between this boundary and the shock have diffused there from the shock. Then dividing the number of particles per unit area of shock between the shock and this boundary, $n_{\mathrm{CR}} k_1/u_1$, by R_{cross} we obtain the average time spent upstream before returning to the shock

$$t_1 \approx \frac{4}{c} \frac{k_1}{u_1}, \tag{26}$$

and hence the cycle time

$$t_{\mathrm{cycle}} \approx \frac{4}{c} \left(\frac{k_1}{u_1} + \frac{k_2}{u_2} \right). \tag{27}$$

The acceleration time at energy E, defined by $E/(dE/dt)$ is then given by

$$t_{\mathrm{acc}} \approx \frac{4}{u_1} \left(\frac{k_1}{u_1} + \frac{k_2}{u_2} \right). \tag{28}$$

We next consider the diffusion for the cases of parallel, oblique, and perpendicular shocks, and estimate the maximum acceleration rate for these cases. The diffusion coefficients required k_1 and k_2 are the coefficients for diffusion parallel to the shock normal. The diffusion coefficient along the magnetic field direction is some factor η times the minimum diffusion coefficient, known as the Bohm diffusion coefficient,

$$k_{\parallel} = \eta \frac{1}{3} r_g c \tag{29}$$

8

where r_g is the gyroradius, and $\eta > 1$.

Parallel shocks are defined such that the shock normal is parallel to the magnetic field ($\vec{B}||\vec{u_1}$). In this case, making the approximation that $k_1 = k_2 = k_\parallel$ and $B_1 = B_2$ one obtains

$$t_{\text{acc}}^\parallel \approx \frac{20}{3}\frac{\eta E}{eB_1 u_1^2}. \tag{30}$$

For a shock speed of $u_1 = 0.1c$ and $\eta = 10$ one obtains an acceleration rate (in SI units) of

$$\left.\frac{dE}{dt}\right|_{\text{acc}} \approx 1.5 \times 10^{-4} ec^2 B. \tag{31}$$

For the oblique case, the angle between the magnetic field direction and the shock normal is different in the upstream and downstream regions, and the direction of the plasma flow also changes at the shock. The diffusion coefficient in the direction at angle θ to the magnetic field direction is given by

$$k = k_\parallel \cos^2\theta + k_\perp \sin^2\theta \tag{32}$$

where $k_\perp$ is the diffusion coefficient perpendicular to the magnetic field. Jokipii [30] shows that

$$k_\perp \approx \frac{k_\parallel}{1 + \eta^2} \tag{33}$$

provided that η is not too large (values in the range up to 10 appear appropriate).

In the case of acceleration at perpendicular shocks, Jokipii [30] has shown that acceleration can be much faster than for the parallel case. For $k_{xx} = k_\perp$ and $B_2 \approx 4B_1$ and one obtains

$$t_{\text{acc}}^\perp \approx \frac{8}{3}\frac{E}{\eta eB_1 u_1^2}. \tag{34}$$

For a shock speed of $u_1 = 0.1c$ and $\eta = 10$ one obtains an acceleration rate (in SI units) of

$$\left.\frac{dE}{dt}\right|_{\text{acc}} \approx 0.04 ec^2 B. \tag{35}$$

This discussion of shock acceleration has been of necessity brief, and has omitted a number of subtleties such as the finite thickness of the shock front, and the reader is referred to the excellent reviews cited earlier for such details. Nevertheless, the basic concepts have been described in sufficient detail that

9

we can consider acceleration and interactions of the highest energy cosmic rays, and to what energies they can be accelerated. Supernova shocks remain strong enough to continue accelerating cosmic rays for about 1000 years. The rate at which cosmic rays are accelerated is inversely proportional to the diffusion coefficient (faster diffusion means less time near the shock). For the maximum feasible acceleration rate, a typical interstellar magnetic field, and 1000 years for acceleration, energies of $10^{14} \times Z$ eV are possible (Z is atomic number) at parallel shocks and $10^{16} \times Z$ eV at perpendicular shocks.

3 Interactions of High Energy Cosmic Rays

Interactions of cosmic rays with radiation and magnetic fields are important both during acceleration when the resulting energy losses compete with energy gains by, for example, shock acceleration, and during propagation from the acceleration region to the observer. For ultra-high energy (UHE) cosmic rays, the most important processes are pion photoproduction and Bethe-Heitler pair production both on the microwave background, and synchrotron radiation. In the case of nuclei, photodisintegration on the microwave background is important. In this section I shall concentrate on photoproduction and pair production.

The mean interaction length, $x_{p\gamma}$, of a proton of energy E is given by,

$$[x_{p\gamma}(E)]^{-1} = \frac{1}{8\beta E^2} \int_{\varepsilon_{\min}}^{\infty} \frac{n(\varepsilon)}{\varepsilon^2} \int_{s_{\min}}^{s_{\max}(\varepsilon,E)} \sigma(s)(s - m_p^2 c^4) ds d\varepsilon, \qquad (36)$$

where $n(\varepsilon)$ is the differential photon number density of photons of energy ε, and $\sigma(s)$ is the appropriate total cross section for the process in question for a centre of momentum (CM) frame energy squared, s, given by

$$s = m_p^2 c^4 + 2\varepsilon E(1 - \beta \cos\theta) \qquad (37)$$

where θ is the angle between the directions of the proton and photon, and βc is the proton's velocity.

For pion photoproduction

$$s_{\min} = (m_p c^2 + m_\pi c^2)^2 \approx 1.16 \text{ GeV}^2, \qquad (38)$$

and

$$\varepsilon_{\min} = \frac{m_\pi c^2 (m_\pi c^2 + 2m_p c^2)}{2E(1 + \beta)} \approx \frac{m_\pi c^2 (m_\pi c^2 + 2m_p c^2)}{4E}. \qquad (39)$$

For photon-proton pair-production the threshold is somewhat lower,

$$s_{\min} = (m_p c^2 + 2m_e c^2)^2 \approx 0.882 \text{ GeV}^2, \qquad (40)$$

10

and

$$\varepsilon_{\min} \approx m_e c^2 (m_e c^2 + m_p c^2)/E. \tag{41}$$

For both processes,

$$s_{\max}(\varepsilon, E) = m_p^2 c^4 + 2\varepsilon E(1 + \beta) \approx m_p^2 c^4 + 4\varepsilon E, \tag{42}$$

and $s_{\max}(\varepsilon, E)$ corresponds to a head-on collision of a proton of energy E and a photon of energy ε.

Examination of the integrand in Equation 36 shows that the energy of the soft photon interacting with a proton of energy E is distributed as

$$p(\varepsilon) = \frac{x_{p\gamma}(E)n(\varepsilon)}{8\beta E^2 \varepsilon^2} \Phi(s_{\max}(\varepsilon, E)) \tag{43}$$

in the range $\varepsilon_{\min} \leq \varepsilon \leq \infty$ where

$$\Phi(s_{\max}) = \int_{s_{\min}}^{s_{\max}} \sigma(s)(s - m_p^2 c^4) ds. \tag{44}$$

Similarly, examination of the integrand in Equation 36 shows that the square of the total CM frame energy is distributed as

$$p(s) = \frac{\sigma(s)(s - m_p^2 c^4)}{\Phi(s_{\max})}, \tag{45}$$

in the range $s_{\min} \leq s \leq s_{\max}$.

The Monte Carlo rejection technique can be used to sample ε and s respectively from the two distributions, and Equation 37 is used to find θ. One then Lorentz transforms the interacting particles to the frame in which the interaction is treated (usually the proton rest frame), and samples momenta of particles produced in the interaction from the appropriate differential cross section by the rejection method. The energies of produced particles are then Lorentz transformed to the laboratory frame, and the final energy of the proton is obtained by requiring energy conservation. In this procedure, it is not always possible to achieve exact conservation of both momentum and energy while sampling particles from inclusive differential cross sections (e.g. multiple pion production well above threshold), and the momentum of the last particle sampled is therefore adjusted to minimize the error.

The mean interaction lengths for both processes, $x_{p\gamma}(E)$, are obtained from Equation 36 for interactions in the microwave background and are plotted as dashed lines in Fig. 4. Dividing by the inelasticity, $\kappa(E)$, one obtains the energy-loss distances for the two processes,

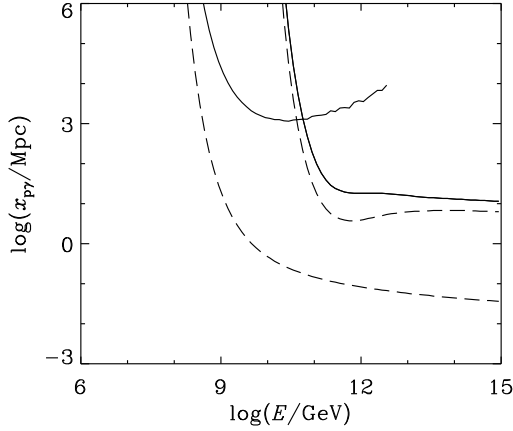$$\frac{E}{dE/dx} = \frac{x_{p\gamma}(E)}{\kappa(E)}. \tag{46}$$

Figure 4: Mean interaction length (dashed lines) and energy-loss distance (solid lines), $E/(dE/dx)$, for proton-photon pair-production and pion-production in the microwave background (lower and higher energy curves respectively). (From Protheroe and Johnson [31]).

4 Maximum Energies

Protons and nuclei can be accelerated to much higher energies than electrons for a given magnetic environment. For stochastic particle acceleration by electric fields induced by motion of magnetic fields B, the rate of energy gain by relativistic particles of charge Ze can be written (in SI units)

$$\left.\frac{dE}{dt}\right|_{\mathrm{acc}} = \xi Z e c^2 B \tag{47}$$

where $\xi < 1$ and depends on the acceleration mechanism; a value of $\xi = 0.04$ might be achieved by first order Fermi acceleration at a perpendicular shock with shock speed $\sim 0.1c$.

4.1 Limits from Synchrotron Losses

The rate of energy loss by synchrotron radiation of a particle of mass Am_p, charge Ze, and energy γmc^2 is

$$-\left.\frac{dE}{dt}\right|_{\mathrm{syn}} = \frac{4}{3}\sigma_T \left(\frac{Z^2 m_e}{Am_p}\right)^2 \frac{B^2}{2\mu_0}\gamma^2 c. \tag{48}$$

12

Equating the rate of energy gain with the rate of energy loss by synchrotron radiation places one limit on the maximum energy achievable by electrons, protons and nuclei:

$$E_e^{\max} \;=\; 6.0 \times 10^2 \xi^{1/2} \left(\frac{B}{1\,\mathrm{T}} \right)^{-1/2} \quad \mathrm{GeV}, \tag{49}$$

$$E_p^{\max} \;=\; 2.0 \times 10^9 \xi^{1/2} \left(\frac{B}{1\,\mathrm{T}} \right)^{-1/2} \quad \mathrm{GeV}, \tag{50}$$

$$E_{Z,A}^{\max} \;=\; 2.0 \times 10^9 \xi^{1/2} \frac{A^2}{Z^{3/2}} \left(\frac{B}{1\,\mathrm{T}} \right)^{-1/2} \quad \mathrm{GeV}. \tag{51}$$

Other limits on the maximum energy are placed by the dimensions of the acceleration region and the time available for acceleration. These limits were obtained and discussed in some detail by Biermann & Strittmatter [32].

4.2   Limits from Interactions with Radiation

Equating the total energy loss rate for proton–photon interactions (i.e. the sum of pion production and Bethe-Heitler pair production) in Fig 4 to the rate of energy gain by acceleration gives the maximum proton energy in the absence of other loss processes. This is shown in Fig 5 as a function of magnetic field which determines the rate of energy gain through Eq. 47. The result is shown by the thin curves for the maximum possible acceleration rate $\xi = 1$ (dashed), plausible acceleration at perpendicular shock $\xi = 0.04$ (solid), and plausible acceleration at parallel shock $\xi = 1.5 \times 10^{-4}$ (dot-dash). Also shown is the maximum energy determined by synchrotron losses (thick lines) for the three cases. As can be seen, for a perpendicular shock it is possible to accelerate protons to $\sim 4 \times 10^{12}$ GeV in a $\sim 10^{-5}$ G field.

In the case of nuclei the situation is a little more complicated. The threshold condition for Bethe-Heitler pair production can be expressed as

$$\gamma > \frac{m_e c^2}{\varepsilon} \left(1 + \frac{m_e}{A m_p} \right), \tag{52}$$

and the threshold condition for pion photoproduction can be expressed as

$$\gamma > \frac{m_\pi c^2}{2\varepsilon} \left(1 + \frac{m_\pi}{2 A m_p} \right). \tag{53}$$

Since $\gamma = E/A m_p c^2$, where A is the mass number, we will need to shift both energy-loss distance curves in Fig. 4 to higher energies by a factor of A. We shall also need to shift the curves up or down as discussed below.
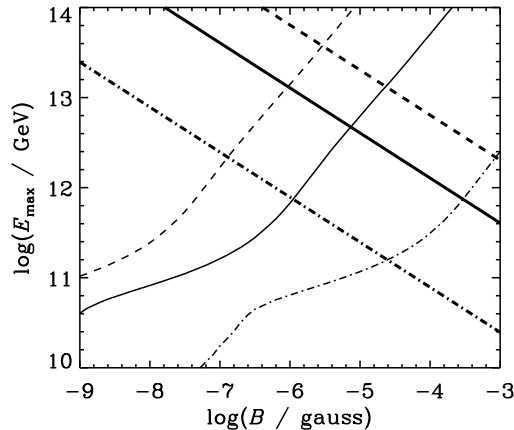
13

Figure 5: Maximum proton energy as a function of magnetic field (see text).

For Bethe-Heitler pair production the energy lost by a nucleus in each collision near threshold is approximately $\Delta E \approx \gamma 2 m_e c^2$. Hence the inelasticity is

$$K \equiv \frac{\Delta E}{E} \approx \frac{2m_e}{Am_p}, \tag{54}$$

and is a factor of A lower than for protons. On the other hand, the cross section goes like Z^2, so the overall shift is down (to lower energy-loss distance) by Z^2/A. For example, for iron nuclei the energy loss distance for pair production is reduced by a factor $26^2/56 \approx 12.1$.

For pion production the energy lost by a nucleus in each collision near threshold is approximately $\Delta E \approx \gamma m_\pi c^2$, and so, as for pair production, the inelasticity is factor A lower than for protons. The cross section increases approximately as $A^{0.9}$ giving an overall increase in the energy loss distance for pion production of a factor $\sim A^{0.1} \approx 1.5$ for iron nuclei.

The energy loss distances for pair production and pion photoproduction, together with the mean free path for pion photoproduction are shown for iron nuclei in Fig. 6. Photodisintegration is very important and has been considered in detail by Tkaczyk W. et al. [33] and Puget et al. [34]. The photodisintegration distance defined by $A/(dA/dx)$ taken from Puget et al. [34] is also shown in Fig. 6. Since iron nuclei will be fragmented also during pion photoproduction, the effective loss distance will be given by the photodisintegration
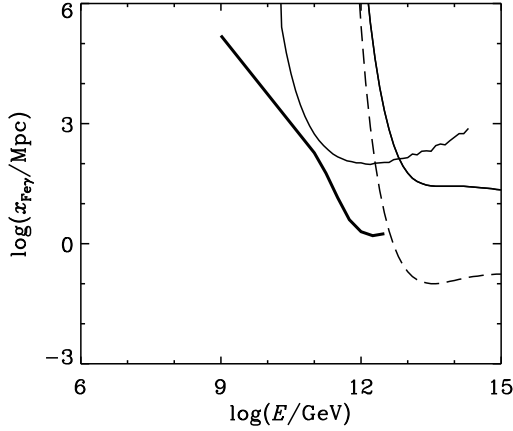
14

Figure 6: Mean interaction length (dashed line) and energy-loss distance (solid line), $E/(dE/dx)$, for Fe-photon pion-production, and energy-loss distance for pair-production in the microwave background (leftmost solid line). Also shown is the photodisintegration distance (thick solid curve).

distance below $\sim 3 \times 10^{12}$ GeV, and by the *mean free path* for pion photoproduction at higher energies. The effective loss distance given in Fig. 6 is used together with the acceleration rate and synchrotron loss rate for iron nuclei to obtain the maximum energy as a function of magnetic field. This is shown in Fig. 7 which is analogous to Fig. 5 for protons. We see that for a perpendicular shock it is possible to accelerate iron nuclei to $\sim 2 \times 10^{13}$ GeV in a $\sim 2 \times 10^{-4}$ G field. While this is higher than for protons, iron nuclei are likely to get photodisintegrated into nucleons of maximum energy 400 EeV, and so there is not much to be gained unless the source is nearby. Of course, potential acceleration sites need to have the appropriate combination of size (much larger than the gyroradius at the maximum energy), magnetic field, and shock velocity (or other relevant velocity), and these criteria have been discussed in detail by Hillas [35].

5   Cascading During Propagation

There are several cascade processes which are important for UHE cosmic rays propagating over large distances through a radiation field: protons interact with photons resulting in pion production and pair production; electrons in-
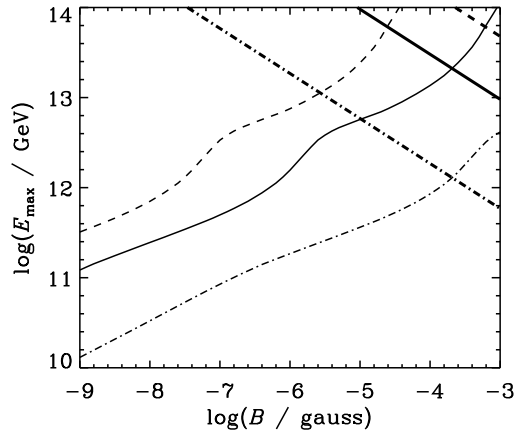
Figure 7: Maximum iron nucleus energy as a function of magnetic field (see Fig. 5).

teract via inverse-Compton scattering and triplet pair production, and emit synchrotron radiation in the intergalactic magnetic field; γ-rays interact by pair production. Energy losses due to cosmological redshifting of high energy particles and γ-rays can also be important, and the cosmological redshifting of the background radiation fields means that energy thresholds and interaction lengths for the above processes also change with epoch (see e.g. Protheroe et al. [36]).

The energy density of the extragalactic background radiation is dominated by that from the cosmic microwave background at a temperature of 2.735 K. Other components of the extragalactic background radiation are discussed in the review of Ressel and Turner [37]. The extragalactic radiation fields important for cascades initiated by UHE cosmic rays include the cosmic microwave background, the radio background and the infrared–optical background. The radio background was measured over twenty years ago [38,39], but the fraction of this radio background which is truly extragalactic, and not contamination from our own Galaxy, is still debatable. Berezinsky [40] was first to calculate the mean free path on the radio background. Recently Protheroe and Biermann [41] have made a new calculation of the extragalactic radio background radiation down to kHz frequencies. The main contribution to the background is from normal galaxies and is uncertain due to uncertainties in their evolution. The mean free path of photons in this radiation field as well as in the

16

microwave and infrared backgrounds is shown in Fig. 8. Also shown is the mean interaction length for muon pair-production which is negligible in comparison with interactions with pair production on the radio background and double pair production on the microwave background.
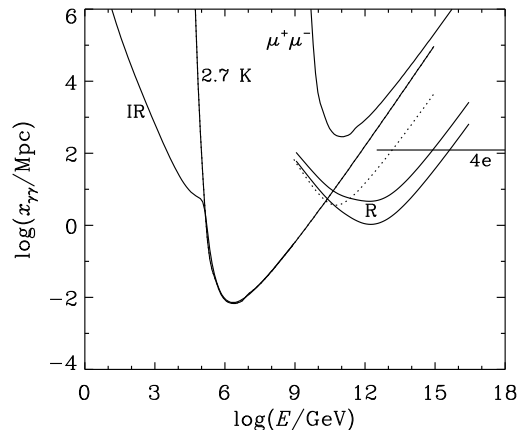

Figure 8: The mean interaction length for pair production for γ-rays in the Radio Background calculated in the present work (solid curves labelled R: upper curve – no evolution of normal galaxies; lower curve – pure luminosity evolution of normal galaxies) and in the radio background of Clark [38] (dotted line). Also shown are the mean interaction length for pair production in the microwave background (2.7K), the infrared and optical background (IR), and muon pair production ($\mu^+\mu^-$) and double pair production (4e) in the microwave background [31]. (From Protheroe and Biermann [41]).

Inverse Compton interactions of high energy electrons and triplet pair production can be modelled by the Monte Carlo technique [42–45], and the mean interaction lengths and energy-loss distances for these processes are given in Fig. 9. Synchrotron losses must also be included in calculations and the energy-loss distance has been added to Fig. 9 for various magnetic fields.

5.1 Practical Aspects of the Cascade

Where possible, to take account of the exact energy dependences of cross-sections, one can use the Monte Carlo method. However, direct application of Monte Carlo techniques to cascades dominated by the physical processes described above over cosmological distances takes excessive computing time. Another approach based on the matrix multiplication method has been de-
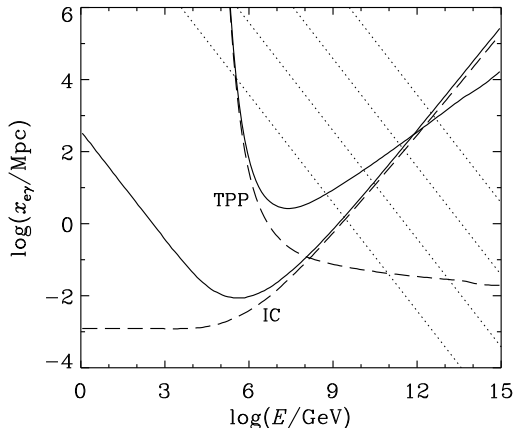
Figure 9: The mean interaction length (dashed line) and energy-loss distance (solid line), $E/(dE/dx)$, for electron-photon triplet pair production (TPP) and inverse-Compton scattering (IC) in the microwave background. The energy-loss distance for synchrotron radiation is also shown (dotted lines) for intergalactic magnetic fields of 10^{-9} (bottom), 10^{-10}, 10^{-11}, and 10^{-12} gauss (top). (From Protheroe and Johnson [31]).

scribed by Protheroe [42] and developed in later papers [31, 46]. A Monte Carlo program is used to calculate the yields of secondary particles due to interactions with radiation, and spectra of produced pions are decayed (e.g. using routines in SIBYLL [47]) to give yields of gamma-rays, electrons and neutrinos. The yields are then used to build up transfer matrices which describe the change in the spectra of particles produced after propagating through the radiation fields for a distance δx. Manipulation of the transfer matrices as described below enables one to calculate the spectra of particles resulting from propagation over arbitrarily large distances.

5.2   Matrix Method

In the work of Protheroe and Johnson [31], fixed logarithmic energy bins were used, and the energy spectra of particles of type α $(\alpha = \gamma, e, p, n, \nu_e, \bar{\nu}_e, \nu_\mu, \bar{\nu}_\mu)$ at distance x in the cascade are represented by vectors $F_j^\alpha(x)$ which give the total number of particles of type α in the jth energy bin at distance x. Transfer matrices, $\mathrm{T}_{ij}^{\alpha\beta}(\delta x)$, give the number of particles of type β in the bin j which result at a distance δx after a particle of type α and energy in bin i initiates a cascade. Then, given the spectra of particles at distance x one can obtain the

18

spectra at distance $(x + \delta x)$

$$F_j^\beta(x + \delta x) = \sum_\alpha \sum_{i=j}^{180} T_{ij}^{\alpha\beta}(\delta x) F_i^\alpha(x) \tag{55}$$

where $F_i^\alpha(x)$ are the input spectra (number in the ith energy bin) of species α.

We could also write this as

$$[F(x + \delta x)] = [T(\delta x)][F(x)] \tag{56}$$

where

$$[F] = \begin{bmatrix} F^\gamma \\ F^e \\ F^p \\ \vdots \end{bmatrix}, \qquad [T] = \begin{bmatrix} T^{\gamma\gamma} & T^{e\gamma} & T^{p\gamma} & \cdots \\ T^{\gamma e} & T^{ee} & T^{pe} & \cdots \\ T^{\gamma p} & T^{ep} & T^{pp} & \cdots \\ \vdots & \vdots & \vdots & \ddots \end{bmatrix}. \tag{57}$$

The transfer matrices depend on particle yields, $Y_{ij}^{\alpha\beta}$, which are defined as the probability of producing a particle of type β in the energy bin j when a primary particle of type α with energy in bin i undergoes an interaction. To calculate $Y_{ij}^{\alpha\beta}$ a Monte Carlo simulation can be used (see Protheroe and Johnson [31] for details).

5.3 Matrix Doubling

From Fig. 9 we see that the smallest effective interaction length is that for synchrotron losses by electrons at high energies. We require δx be much smaller than this distance which is of the order of parsecs for the highest magnetic field considered. To follow the cascade for a distance corresponding to a redshift of $z \sim 9$, and to complete the calculation of the cascade using repeated application of the transfer matrices would require $\sim 10^{12}$ steps. This is clearly impractical, and one must use the more sophisticated approach described below.

The matrix method and matrix doubling technique have been used for many years in radiative transfer problems [48, 49]. The method described by Protheroe and Stanev [46] is summarized below. Once the transfer matrices have been calculated for a distance δx, the transfer matrix for a distance $2\delta x$ is simply given by applying the transfer matrices twice, i.e.

$$[T(2\delta x)] = [T(\delta x)]^2. \tag{58}$$

In practice, it is necessary to use high-precision during computation (e.g. double-precision in FORTRAN), and to ensure that energy conservation is

preserved after each doubling. The new matrices may then be used to calculate the transfer matrices for distance $4\delta x$, $8\delta x$, and so on. A distance $2^n\delta x$ only requires the application of this 'matrix doubling' n times. The spectrum of electrons and photons after a large distance Δx is then given by

$$[\mathrm{F}(x + \Delta x)] = [\mathrm{T}(\Delta x)][\mathrm{F}(x)] \tag{59}$$

where $[\mathrm{F}(x)]$ represents the input spectra, and $\Delta x = 2^n\delta x$. In this way, cascades over long distances can be modelled quickly and efficiently.

6 The Origin of Cosmic Rays between 100 TeV and 300 EeV

The subject of the origin of cosmic rays at these energies has been reviewed [35, 50], and one of the very few plausible acceleration sites may be associated with the radio lobes of powerful radio galaxies, either in the hot spots [51] or possibly the cocoon or jet [52]. One-shot processes comprise another possible class of sources [53, 54].

Acceleration at the termination shock of the galactic wind from our Galaxy has been also been suggested [55], but due to the lack of any statistically significant anisotropy associated with the Galaxy is unlikely to be the explanation. However, a very recent re-evaluation of the world data set of cosmic rays has shown that there is a correlation of the arrival directions of cosmic rays above 40 EeV with the supergalactic plane [56], lending support to an extragalactic origin above this energy, and in particular to models where "local" sources (< 100 Mpc) would appear to cluster near the supergalactic plane (e.g. powerful radio galaxies as in the model of Rachen and Biermann [51].

Rachen and Biermann [51] have demonstrated that cosmic ray acceleration in Fanaroff-Riley Class II radio galaxies can fit the observed spectral shape and the normalization at $10 - 100$ EeV to within a factor of less than 10. The predicted spectrum below this energy also fits the proton spectrum inferred from Fly's Eye data [57]. Protheroe and Johnson [31] have repeated Rachen and Biermann's calculation to calculate the flux of diffuse neutrinos and gamma rays which would accompany the UHE cosmic rays, and their result is shown in Fig. 10.

6.1 Observability of Ultra High Energy Gamma Rays

Above 100 EeV the interaction properties of gamma rays in the terrestrial environment are very uncertain. Two effects may play a significant role: interaction with the geomagnetic field, and the Landau-Pomeranchuk-Migdal (LPM) effect [59, 60].
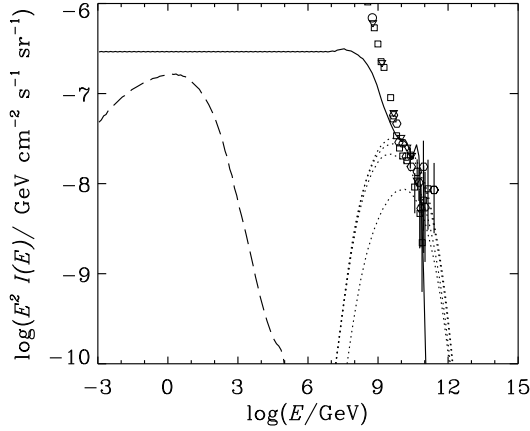
Figure 10: Cosmic ray proton intensity multiplied by E^2 in the model of Rachen and Biermann for $H_0 = 75$ km s^{-1} Mpc^{-1} with proton injection up to 3×10^{11} GeV (solid line). Also shown are intensities of neutrinos (dotted lines, $\nu_\mu, \bar{\nu}_\mu, \nu_e, \bar{\nu}_e$ from top to bottom), and photons (long dashed lines). Data are from Stanev [58]; large crosses at EeV energies are an estimate of the proton contribution to the total intensity based on Fly's Eye observations. (From Protheroe and Johnson [31]).

Energetic gamma rays entering the atmosphere will be subject to the LPM effect (the suppression of electromagnetic cross-sections at high energy) which becomes very important at ultra-high energies. The radiation length changes as $(E/E_{\mathrm{LPM}})^{1/2}$, where $E_{\mathrm{LPM}} = 6.15 \times 10^4 \ell_{\mathrm{cm}}$ GeV, and ℓ_{cm} is the standard Bethe-Heitler radiation length in cm [61]. Protheroe and Stanev [62] found that average shower maximum will be reached below sea level for energies 5×10^{11} GeV, 8×10^{11} GeV, and 1.3×10^{12} GeV for gamma–rays entering the atmosphere at $\cos\theta = 1$, 0.75, and 0.5 respectively. Such showers would be very difficult to reconstruct by experiments such as Fly's Eye and at best would be assigned a lower energy.

Before entering the Earth's atmosphere gamma rays and electrons are likely to interact on the geomagnetic field (see Erber [63] for a review of the theoretical and experimental understanding of the interactions). In such a case the gamma rays propagating perpendicular to the geomagnetic field lines would cascade in the geomagnetic field, i.e. pair production followed by synchrotron radiation. The cascade process would degrade the gamma ray energies to some extent (depending on pitch angle), and the atmospheric cascade would then be generated by a bunch of gamma-rays of lower energy. Aharonian et al. [64]

21

have considered this possibility and conclude that this bunch would appear as one air shower made up of the superposition of many air showers of lower energy, where the LPM effect is negligible; the air shower having the energy of the initial gamma-ray outside the geomagnetic field. If this is the case, then gamma rays above 300 EeV would be observable by Fly's Eye, etc. There is however, some uncertainty as to whether pair production will take place in the geomagnetic field. This depends on whether the geomagnetic field spatial dimension is larger than the formation length of the electron pair, i.e. the length required to achieve a separation between the two electrons that is greater than the classical radius of the electron (see also Stanev and Vankov [65]).

7 Exotic Origin Models

We now discuss the possibility that the highest energy cosmic rays are not single nucleons. Obvious candidates are heavier nuclei (e.g. Fe), γ-rays, and neutrinos. In general it is even more difficult to propagate nuclei than protons, because of the additional photonuclear disintegration which occurs [33,34,66]. The possibility that the 300 EeV event is a γ-ray has been discussed recently [67] and, although not completely ruled out, the air shower development profile seems inconsistent with a γ-ray primary. Weakly interacting particles such as neutrinos will have no difficulty in propagating over extragalactic distances, of course. This possibility has been considered, and generally discounted [66,67], mainly because of the relative unlikelihood of a neutrino interacting in the atmosphere, and the necessarily great increase in the luminosity required of cosmic sources. Magnetic monopoles accelerated by magnetic fields in our Galaxy have also been suggested [68] and can not be ruled out as the highest energy events until the expected air shower development of a monopole-induced shower is worked out.

7.1 Topological Defect Origin

One exciting possible explanation of the highest energy cosmic rays is the topological defect (TD) scenario [69–71], where the observed cosmic rays are a result of top-down cascading, from somewhat below GUT scale energy, $\sim 10^{16}$ GeV, to 10^{11} GeV and lower energies. Generally, these models put out much of the energy in a very flat spectrum of photons and electrons extending up to the mass of "X–particles" emitted which may be lower than 10^{16} GeV, depending on the theory. Approximating this spectrum by a monoenergetic injection of photons of energy 10^{15} GeV, Protheroe & Johnson [31] showed that spectra from single TD sources can not explain the 3×10^{11} GeV events.

22

The main problem with topological defect models is the wide range of model parameters in which this scenario could, in principle, be applied. This is very different from astrophysical scenarios [51] where nearly all of the properties of the astrophysical objects are restricted from observations (luminosities at different wavelengths, magnetic field, etc.). Parameters of TD scenarios include: mass of the X–particle (maximum injection energy for X–particle decay products), energy spectra and final state composition of the decay products, and cosmological evolution of the topological defect injection rate [72, 73].

To compare the TD decay products with the cosmic ray data one has to study the change of the spectra during propagation [31, 73]. This problem is more severe than for the case of "bottom-up" scenarios because most of the energy from X–particle decay, and subsequent decays, emerges in electrons, photons and neutrinos, with only about 3% in nucleons. The electrons and photons initiate electromagnetic cascades in the extragalactic radiation fields and magnetic field, resulting in a complicated spectrum of electrons and photons which is very sensitive to the radiation and magnetic environment. For example, recently the HEGRA group [74] have placed an upper limit on the ratio of gamma-rays to cosmic rays of $\sim 10^{-2}$ at 10^5 GeV, and based on a TD model calculation [69] which neglected the IR background and gave a higher ratio argued that TD models were ruled out. However, inclusion of the IR reduces the 10^5 GeV gamma-ray intensity to below the HEGRA limit.

Unfortunately, many of the relevant parameters of extragalactic space (average magnetic field, strength of the radio and IR/optical backgrounds) are not well known. Protheroe and Johnson [75] have considered one set of parameters ($m_X c^2 = 10^{15}$ GeV, constant injection per co-moving volume, $B = 10^{-9}$ gauss) and rule out TD as the origin of the 3×10^{11} GeV events. More recently, Lee [73] and Sigl, Lee and Coppi [76], adopting a probably unphysical lower X–particle mass $m_X c^2 = 10^{14}$ GeV (the X–particle mass is expected to be near the unification mass which is $10^{16.0 \pm 0.3}$ GeV [77]), and a lower magnetic field claim the TD scenario is not ruled out. However, Protheroe and Stanev [62] argue that these X–particles masses are ruled out as well. The details are not simple, and include considering whether or not UHE gamma rays in the cascade are observable or not by air shower arrays, but in either case TD models appear to be ruled out *as the origin of the 300 EeV events.*

8 Conclusion

While the origin of the highest energy cosmic rays remains uncertain, there appears to be no necessity to invoke exotic models. Shock acceleration, which is believed to be responsible for the cosmic rays up to at least 100 GeV, is a

well-understood mechanism and there is evidence of shock acceleration taking place in radio galaxies [32], and the conditions there are favourable for acceleration to at least 300 EeV. Such a model, in which cosmic rays are accelerated in Fanaroff-Riley Class II radio galaxies, can readily account for the flat component of cosmic rays which dominates the spectrum above ~ 10 EeV [57]. Indeed, one of the brightest FR II galaxies, 3C 134, is a candidate source for the 300 EeV Fly's Eye event (P.L. Biermann, personal communication).

Whatever the source of the highest energy cosmic rays, because of their interactions with the radiation and magnetic fields in the universe, the cosmic rays reaching Earth will have spectra, composition and arrival directions affected by propagation. Many of the important parameters, e.g. extragalactic magnetic fields and radiation fields, are uncertain, and more work is needed to obtain better estimates of these and thereby help unravel the puzzle. When better information is available, and good statistics on the arrival directions, energy spectra and composition, as well as the intensity of the diffuse background of very high energy gamma rays (partly produced in cascades initiated by cosmic ray interactions), we will be better placed to understand the origin of the highest energy particles occurring in nature. The Auger Project, an international collaboration to build two UHE cosmic ray detectors, one in the United States and one in Argentina, each having a collecting area in excess of 1000 km^2 (see the lecture by J.M. Matthews in this volume), will go a long way to help answer these questions.

Acknowledgments

References

1. Lagage, P.O., and Cesarsky, C.J., *Astron. Astrophys.* **118** (1983) 223
2. Drury, L.O'C., Aharonian, F.A., and Völk, H.J., *Astron. Astrophys.* **287** (1994) 959.
3. Gaisser, T.K., Protheroe, R.J., and Stanev, T., *Astrophys. J.* submitted (1996) astro-ph/9609044.
4. Esposito, J.A., Hunter, S.D., Kanbach, G., and Sreekumar, P., *Astrophys. J.* **461** (1996) 820.

5. Brazier, K.T.S., Kanbach, G., Carraminana, A., Guichard, J., and Merck, M., *Mon. Not. R. Astr. Soc.*, **281** (1996) 1033.

6. Koyama, K., Petre, R., Gotthelf, E.V., Hwang, U., Matsuura, M., Ozaki, M., and Holt, S.S., *Nature* **378** (1995) 255.

7. Reynolds, S.P., *Astrophys. J. Lett.* **459** (1996) L13.

8. Mastichiadis, A., *Astron. Astrophys.*, **305** (1996) 53.

9. Donau, A.C., and Biermann, P.L., *Astron. Astrophys.* submitted (1996).

10. Markiewicz W.J., Drury L. O'C., and Volk H.J., *Astron. Astrophys.* **236** (1990) 487.

11. Axford W.I. *Astrophysical Aspects of Cosmic Rays* ed. M. Nagano and F. Takahara (World Scientific, Singapore, 1991) p. 46.

12. Ip, W.-H., and Axford, W.I., in *Particle Acceleration in Cosmic Plasmas*, eds. T.K. Gaisser and G.P. Zank (AIP Conference Proceedings No. 264, 1991) p. 400.

13. Biermann, P.L., and Cassellini, J.P., *Astron. Astrophys.* **277** (1993) 691.

14. Bird, D.J., *et al.*, *Ap. J.* **424** (1994) 491.

15. Hayashida, N., *et al.*, *Phys. Rev. Lett.* **73** (1994) 3491.

16. Bird, D.J., *et al.*, *Ap. J.* **441** (1995) 144.

17. Greisen, K., *Phys. Rev. Lett.* **16** (1966) 748.

18. Zatsepin, G.T., and Kuz'min, V.A., *JETP Lett.* **4** (1966) 78.

19. Hill, C.T., and Schramm, D.N., *Phys. Rev. D* **31** (1985) 564.

20. Berezinsky, V.S. and Grigor'eva, S.I., *Astron. Astrophys.* **199** (1988) 1.

21. Gaisser, T.K., *Cosmic Rays and Particle Physics*, (Cambridge University Press, Cabridge, 1990).

22. Drury, L.O'C., *Space Sci. Rev.* **36** (1983) 57.

23. Blandford, R, and Eichler, D., *Phys. Rep.* **154** (1987) 1.

24. Berezhko, E.G., and Krymski, G.F., *Usp. Fiz. Nauk* **154** (1988) 49.

25. Jones, F.C., and Ellison, D.C., *Space Sci. Rev.* **58** (1991) 259.

26. Axford, W.I., Lear, E., and Skadron, G., *Proc. 15th Int. Cosmic Ray Conf., Plovdiv*, **11** (1977) 132.

27. Krymsky, G.F., *Dokl. Akad. Nauk. SSSR*, **243** (1977) 1306.

28. Bell, A.R., *Mon. Not. R. Astr. Soc.*, **182** (1978) 443.

29. Blandford, R.D., and Ostriker, J.P., *Astrophys. J. Lett.* **221** (1978) L29.

30. Jokipii, J.R., *Astrophys. J.* **313** (1987) 842.

31. Protheroe, R.J., and Johnson, P.A., *Astroparticle Phys.* **4** (1995) 253 and erratum **5** (1996) 215.

32. Biermann, P.L., and Strittmatter, P.A., *Ap. J.* **322** (1987) 643.

33. Tkaczyk, W., Wdowczyk, J., and Wolfendale, A.W., *J. Phys. A* **8** (1975)

1518.

34. Puget, J.L., Stecker, F.W., Bredekamp, J.H., *Ap. J.* **205** (1976) 638.

35. Hillas, A.M, *Ann. Rev. Astron. Astrophys.* **22** (1984) 425.

36. Protheroe, R.J., Stanev, T., and Berezinsky, V.S., *Phys. Rev. D15*, **151** (1995) 4134.

37. Ressell, M.T., and Turner, M.S., *Comm. Astrophys.* **14** (1990) 323.

38. Clarke, T.A., Brown, L.W. and Alexander, J.K., *Nature* **228** (1970) 847.

39. Bridle, A.H., *Mon. Not. R. Astron. Soc.* **136** (1967) 14.

40. Berezinsky, V.S., *Yad. Fiz.* **11** (1970) 339; English translation in *Sov. J. Nucl. Phys.*, **11** (1970) 222.

41. Protheroe, R.J., and Biermann, P.L., *Astrparticle Phys.*, in press (1996) astro-ph/9605119.

42. Protheroe, R.J., *Mon. Not. R. Astron. Soc.* **221** (1986) 769.

43. Protheroe, R.J., *Mon. Not. R. Astr. Soc.* **246** (1990) 628.

44. Protheroe, R.J., Mastichiadis A. and Dermer C.D. *Astroparticle Phys.* **1** (1992) 113.

45. Mastichiadis, A., Protheroe, R.J. and Szabo, A.P. *Mon. Not. R. Astron. Soc.* **266** (1994) 910.

46. Protheroe, R.J., and Stanev, T.S., *Mon. Not. R. Astron. Soc.* **264** (1993) 191.

47. Fletcher, R.S., Gaisser, T.K., Lipari, P., Stanev, T., *Phys. Rev. D* **50** (1994) 5710.

48. van de Hulst, H.C., *A New Look at Multiple Scattering*, Report, NASA Institute for Space Studies, New York, 1963).

49. Hovenier, J.V., *Astron. Astrophys.* **13** (1971) 7.

50. Axford, W.I., *Ap. J. Suppl.* **90** (1994) 937.

51. Rachen, J.P., and Biermann, P.L., *Astron. Astrophys.* **272** (1993) 161.

52. Norman, C.A., Melrose, D.B., and Achterberg, A., *Astrophys. J.* **454** (1995) 60.

53. Haswell, C.A., Tajima, T., and Sakai, J.-L., *Ap. J.* **401** (1992) 495.

54. Sorrell, W.H., *Ap. J.* **323** (1987) 647.

55. Jokipii, J.R., and Morfill G.E., *Ap. J. Lett.* **290** (1985) L1.

56. Stanev, T., Biermann, P.L., Lloyd-Evans, J., Rachen, J.P., and Watson, A.A., *Phys. Rev. Lett.* **75** (1995) 3056.

57. Rachen, J.P., Stanev, T., and Biermann, P.L., *Astron. Astrophys.* **273** (1993) 377.

58. Stanev, T., in *Particle Acceleration in Cosmic Plasmas*, edited by G.P. Zank and T.K. Gaisser (American Institute of Physics, New York, 1992) p. 379.

59. Landau, L.D., and Pomeranchuk, I., *Dok. Akad. Nauk. SSSR* **92** (1953)

535.

60. Migdal, A.B., *Phys. Rev.* **103** (1956) 1811.

61. Stanev, T., et al., *Phys. Rev. D* **25** (1982) 1291.

62. Protheroe, R.J., and Stanev, T., *Phys. Rev. Lett.* **77** (1996) 3708.

63. Erber, T., *Phys. Rev.* **38** (1968) 626.

64. Aharonian, F.A., Kanevsky, B.L., and Sahakian, J., *J. Phys. G*, **17** (1991) 1909.

65. Stanev, T., and Vankov, H.P., *Phys. Rev. D.* submitted (1996) astro-ph/9607011.

66. Elbert, J.W., and Sommers, P., *Ap. J.* **441** (1995) 151.

67. Halzen F., Vazquez R.A., Stanev T. and Vankov H.P., *Astroparticle Phys.*, **3** (1995) 151.

68. Kephart, T.W., and Weiler, T.J., *Astroparticle Phys.*, **4** (1996) 271.

69. Aharonian, F.A., Bhattacharjee, P., and Schramm, D., *Phys. Rev. D* **46** (1992) 4188

70. Bhattacharjee, P., Hill, C.T., and Schramm, D.N., *Phys. Rev. Lett.* **69** (1992) 567.

71. Gill, A.J., and Kibble, T.W.B., *Phys. Rev. D* **50** (1994) 3660.

72. Sigl, G., *Space Sci. Rev.* **75** (1996) 375.

73. Lee, S., *Phys. Rev D* submitted (1996) astro-ph/9604098.

74. Karle, A., *Phys. Lett. B*, **347** (1995) 161.

75. Protheroe, R.J., and Johnson, P.A., "Phenomenological Aspects of Underground Physics (TAUP95)", ed. M. Fratas, *Nucl. Phys. B., Proc. Suppl.*, **48** (1996) 485.

76. Sigl, G., Lee, S., and Coppi, P., *Phys. Rev. Lett.* in press (1996) astro-ph/9604093.

77. Amaldi, U., de Boer, W., and Fürstenau, H., *Phys. Lett.* **B260** (1991) 447.